a-Si:H/μc-Si:H tandem junction based photocathodes with high open-circuit voltage for efficient hydrogen production

Félix Urbain,[a] Vladimir Smirnov, Jan-Philipp Becker, Uwe Rau, and Friedhelm Finger
IEK-5 Photovoltaik, Forschungszentrum Jülich, Jülich D-52425, Germany

Jürgen Ziegler, Bernhard Kaiser, and Wolfram Jaegermann
Institute of Materials Science, TU Darmstadt, Darmstadt D-64287, Germany

(Received 16 June 2014; accepted 8 October 2014)

Thin film silicon tandem junction solar cells based on amorphous silicon (a-Si:H) and microcrystalline silicon (μc-Si:H) were developed with focus on high open-circuit voltages for the application as photocathodes in integrated photoelectrochemical cells for water electrolysis. By adjusting various parameters in the plasma enhanced chemical vapor deposition process of the individual μc-Si:H single junction solar cells, we showed that a-Si:H/μc-Si:H tandem junction solar cells exhibit open-circuit voltage over 1.5 V with solar energy conversion efficiency of 11% at a total silicon layer thickness below 1 μm. Our approach included thickness reduction, controlled SiH_4 profiling, and incorporation of intrinsic interface buffer layers. The applicability of the tandem devices as photocathodes was evaluated in a photoelectrochemical cell. The a-Si:H/μc-Si:H based photocathodes exhibit a photocurrent onset potential of 1.3 V versus RHE and a short-circuit photocurrent of 10.0 mA/cm^2. The presented approach may provide an efficient and low-cost pathway to solar hydrogen production.

I. INTRODUCTION

Solar-assisted hydrogen production via water splitting by integrated semiconductor based photoelectrochemical systems holds great promise as a cost-effective, environmentally benign energy concept and has been attracting keen interest among many research groups.[1,2] Recently, the development of photoelectrodes has been extensively pushed forward, which has led to a vast variety of photoelectrode material systems for water splitting.[3] Efficient conversion of solar energy into a chemical fuel in the form of hydrogen requires photoelectrodes, which generate a photovoltage well above 1.23 V, which is the minimum potential difference to drive the water splitting reactions (disregarding overpotential losses) at a high photocurrent, which defines the amount of produced molecular hydrogen.[4,5] To date, solar-to-hydrogen efficiencies for integrated water splitting devices over 10% efficiency have been reported only for expensive and chemical unstable III–V photoelectrode materials in two-junction devices[6–8] or photovoltaic-electrolysis devices based on CIGS ($CuIn_xGa_{1-x}Se_2$).[9] Among alternative candidates, thin film silicon-based photoelectrodes have strongly emerged in recent years.[10–15] In fact, silicon-based thin film technology presents a promising pathway to sustainable solar hydrogen production due to its earth abundance, low cost, and nontoxicity.[16]

Whereas former studies, listed above,[10–14] exclusively focused on thin film amorphous silicon multijunction devices for water splitting, this study reports on the development and utilization of thin film silicon tandem junction photocathodes made of hydrogenated amorphous silicon (a-Si:H) and hydrogenated microcrystalline silicon (μc-Si:H). In contrast to a-Si:H/a-Si:H tandem junction solar cells, which suffer from rather low photocurrents, the combination of a-Si:H and μc-Si:H in tandem junction devices allows for a more efficient utilization of the solar spectrum and therefore for the generation of higher photocurrents. Additionally, a-Si:H/μc-Si:H tandem devices show less light induced degradation than its all-amorphous counterparts.[17,18] However, as a-Si:H has a higher electronic band gap than μc-Si:H, the photovoltage is increased for amorphous silicon multijunctions. Accordingly, there is a tradeoff between high photovoltages and high photocurrents.

To close this high photovoltage/high photocurrent gap, the purpose of this study is to develop a-Si:H/μc-Si:H tandem devices focusing on the improvement of the open-circuit voltage (V_{OC}) without significantly impairing the short-circuit current (J_{SC}), and thus the conversion efficiency of the device. To do so, we first investigated

[a]Address all correspondence to this author.
e-mail: f.urbain@fz-juelich.de
This paper has been selected as an Invited Feature Paper.
DOI: 10.1557/jmr.2014.308

the ways to increase V_{OC} in μc-Si:H single junction solar cells and subsequently implemented μc-Si:H subcells with improved V_{OC} in tandem junction a-Si:H/μc-Si:H cells. The improvement in the performance of single junction μc-Si:H solar cells was conducted by the following routes: (i) variation in the intrinsic μc-Si:H absorber layer thickness; (ii) control of the SiH_4 flow during deposition of the intrinsic μc-Si:H absorber layer, aiming to maintain a low crystallinity growth across the entire i-layer; and (iii) incorporation of an intrinsic amorphous buffer layer at the n–i interface of the μc-Si:H solar cell. As a result, V_{OC} of the μc-Si:H single junction solar cells could considerably be improved by around 100 mV up to a value of 580 mV.

Furthermore, based on (photo-)electrochemical experiments, the performance of the developed a-Si:H/μc-Si:H tandem junction photocathodes was evaluated with respect to the hydrogen evolution reaction (HER) and compared to an a-Si:H/a-Si:H photocathode.

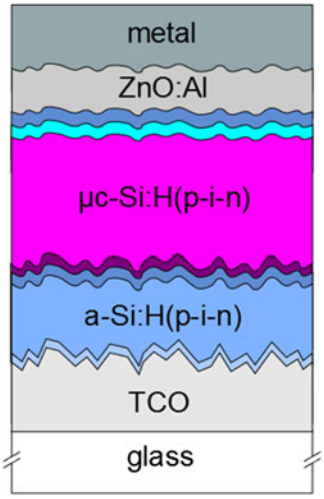

FIG. 1. Schematic drawing of the layer stack of a-Si:H/μc-Si:H tandem solar cells.

II. EXPERIMENTAL DETAILS

A. Preparation of a-Si:H and μc-Si:H layers and solar cells

All thin film silicon layers (a-Si:H and μc-Si:H) were deposited by a plasma enhanced chemical vapor deposition technique in a multi chamber system. For the intrinsic absorber layers, a mixture of silane (SiH_4) and hydrogen (H_2) gases was used. For the n- and p-type layers, trimethylborane (TMB), methane (CH_4) and phosphine (PH_3) gases were added to the silane–hydrogen mixture. μc-Si:H solar cells were fabricated with an μc-Si:H p-type layer, an intrinsic μc-Si:H absorber layer and an a-Si:H n-type layer. For μc-Si:H p-type and intrinsic layer depositions, an excitation frequency of 94.7 MHz was applied. For all a-Si:H layers, an excitation frequency of 13.56 MHz was applied. Single junction and tandem junction solar cells were made in a p–i–n and in a p–i–n–p–i–n superstrate configurations, respectively, with a sputtered zinc oxide/silver (ZnO:Al/Ag) reflecting rear contact[19] defining the area (1 cm^2) of the individual cells. For the a-Si:H/μc-Si:H tandem device, the absorber layer thickness of the μc-Si:H bottom cell was varied between 450 and 1300 nm and the a-Si:H top cell thickness was accordingly adjusted between 400 and 100 nm with a silane concentration (SC) of 4%, defined as the ratio between the SiH_4 flow and the total gas flow. The p- and n-type layers are the same for all fabricated solar cells and are deposited at a substrate temperature (T_S) of 180 °C. The substrate temperature for the μc-Si:H and a-Si:H absorber layers was 180 and 130 °C, respectively.[20] Amorphous intrinsic buffer layers were deposited with a SC of 10% and a T_S of 180 °C. Single and tandem junction solar cells were deposited on 100 cm^2 textured aluminum-doped ZnO coated glass substrates. Figure 1 schematically shows the a-Si:H/μc-Si:H tandem junction solar cell configuration used in the photovoltaic (PV) arrangement. For the photoelectrochemical arrangement, 50 nm of platinum was deposited on the ZnO:Al/Ag back contact by electron beam evaporation. This layer is intended to act as a catalyst on the electrolyte side.

B. Characterization of materials and solar cells

The structural properties of intrinsic μc-Si:H absorber layers were probed using Raman spectroscopy (λ = 532 nm and λ = 488). The ratio of integrated intensities attributed to crystalline and amorphous regions, $I_C^{RS} = I_C/(I_C + I_a)$, was used as semiquantitative value of the crystalline volume fraction.[21] Samples were characterized either by a laser beam (λ = 532) directed on the as-produced sample, or, for selected samples, the Raman intensity ratio depth profile of the structure of the intrinsic absorber layer along the growth axis was determined by a gradient etching method (λ = 488 nm).[22,23] Here, Raman scattering measurements were carried out on slantwise etched craters through the solar cell structure.

Solar cells were characterized by current–voltage (*J–V*) measurements at standard test conditions (AM 1.5 G, 100 mW/cm^2, 25 °C) illumination using a double source (Class A) AM 1.5 sun simulator. Furthermore, spectral response measurements [quantum efficiency (QE)] of the tandem solar cells were measured using a monochromator as a light source in the wave length range between 300 and 1100 nm. The top and bottom cell QEs were separately determined using a spectrally filtered bias light from a tungsten lamp. Additional details on QE setup can be found in Ref. 24.

C. Photoelectrochemical measurements

The photoelectrochemical performance of the photocathodes was evaluated at room temperature in an

aqueous 0.1 M sulfuric acid (H_2SO_4) solution using a three-electrode configuration.[25] The potential of the working electrode was controlled by a potentiostat (Metrohm, μAutolab Type III). White light photocurrent measurements were performed under simulated AM1.5 solar illumination (100 mW/cm^2) using an Oriel LCS-100 solar simulator (model 94011A, Newport Corporation, Irvine, CA). The solar cells were illuminated through the glass substrate. The setup of the electrochemical cell (type Zahner PECC-2) consists of a Teflon cell body and three electrodes: a working electrode (optimized a-Si:H/μc-Si:H tandem junction solar cell, 8 mm diameter), a coiled platinum wire as a counter electrode, and a Ag/AgCl reference electrode in contact with 3 M sodium chloride (NaCl) [0.268 V versus normal hydrogen electrode (NHE)]. For simplicity, the entire setup will be denoted as a photoelectrochemical cell (PEC) arrangement hereafter. Linear sweep voltammetry measurements were performed with a scan rate of 30 mV s^{-1}. Electrical contact to the transparent conductive oxide (TCO) coated substrate, i.e., the front contact of the solar cell, was made by a silver paste. The PEC arrangement (three-electrode configuration) is schematically shown in Fig. 2.

III. RESULTS

A. Solar cells

1. μc-Si:H single junction solar cells

Since the open-circuit voltage (V_{OC}) of μc-Si:H solar cells correlates with the crystallinity of the absorber material,[26–28] Raman spectroscopy measurements were conducted to estimate the crystalline volume fraction in the samples. The crystallinity I_C^{RS} is mainly controllable through the SC ratio during growth of the μc-Si:H layer. As expected, I_C^{RS} strongly decreases with increasing SC of the intrinsic μc-Si:H absorber layer (Fig. 3).

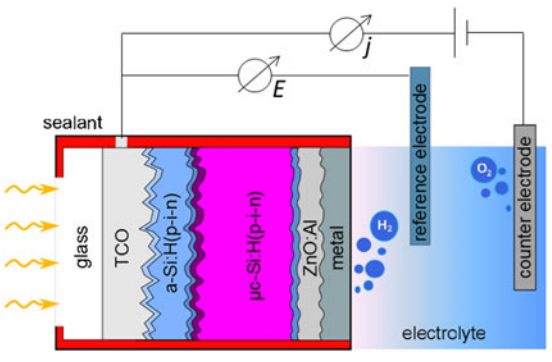

FIG. 2. Schematic drawing of the photoelectrochemical cell (PEC) measurement setup (three electrode configuration). The components are the a-Si:H/μc-Si:H photocathode (working electrode), the reference electrode (Ag/AgCl electrode in contact with 3 M NaCl), the electrolyte (0.1 M H_2SO_4), and the counter electrode (coiled platinum wire).

a. Thickness variation of the μc-Si:H absorber layer

The performance of the μc-Si:H solar cells, with respect to V_{OC} as a function of the evaluated crystallinity of the absorber layers is presented in Fig. 4 for the solar cells with absorber layer thickness of 1300, 650, and 450 nm. It is well accepted that a decrease in I_C^{RS}, i.e., an increase in SC, leads to an increase in V_{OC} because the material increasingly becomes amorphous.[26] For 1300 nm thick μc-Si:H absorber layers, the data show that from I_C^{RS} of 15–70% there was only a weak effect on V_{OC}. In this region, the data points show a curvature and V_{OC} varied between 490 and 530 mV with a V_{OC} maximum at 50–40% crystallinity. A strong increase in V_{OC} from 530 to 620 mV was visible only for I_C^{RS} values below 15%. A similar trend of V_{OC} as a function of SC for thick μc-Si:H absorber layers above 1.5 μm was already reported in Ref. 27. By reducing the thickness of the μc-Si:H absorber layer to 650 and 450 nm, respectively, the general trend indicates that V_{OC} increases for a given crystallinity as shown in

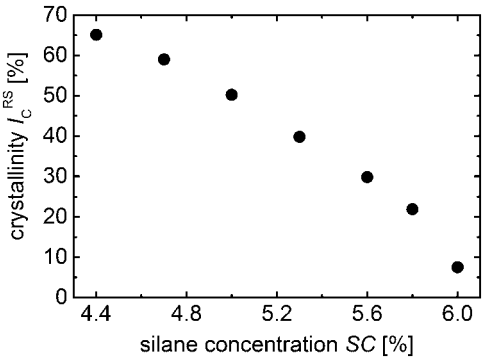

FIG. 3. Crystallinity I_C^{RS} as a function of the SC of the intrinsic μc-Si:H absorber layer.

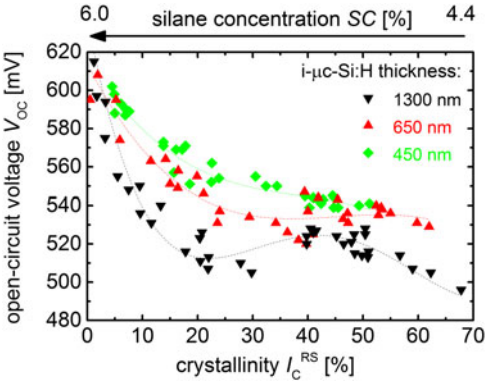

FIG. 4. Open-circuit voltage V_{OC} of μc-Si:H single junction solar cells as a function of the crystallinity I_C^{RS} of the intrinsic μc-Si:H absorber layers (arrow on the upper *x*-axis illustrates the corresponding trend for SC). Absorber layer thicknesses of 1300 nm (black triangles), 650 nm (red triangles), and 450 nm (green diamonds) were investigated. The dashed lines serve as a guide to the eye.

Fig. 4. Overall, our results indicate that thinner absorber layers tend to increase the V_{OC} values, especially in the moderate crystallinity range. For example, at the I_C^{RS} of around 30%, V_{OC} increases by around 60 mV (from 500 to 560 mV) when the absorber layer is reduced from 1300 to 450 nm.

b. SiH_4 profiling

This section focuses on the growth control of the μc-Si:H absorber layer by means of SiH_4 profiling, aiming to obtain a moderate crystallinity (around 50%) absorber layer across the entire i-layer. Previous studies show that profiling could lead to improved performance.[29,30] Figure 5 depicts the Raman intensity ratio depth profile of the structure of the μc-Si:H solar cell along the growth axis, including n- and p-type layers and the intrinsic 1300 nm thick absorber layer (indicated by dashed lines). First, a μc-Si:H solar cell deposited with a standard deposition process (SC of 4.4 and 5%) was investigated. The corresponding SC profile (change of SC during deposition time) is shown in the supplementary material (Fig. S1). The corresponding Raman depth profile is presented in Fig. 5. To a cell thickness of 1000 nm, I_C^{RS} consistently increases from 42% to 70% and decreases again down to around 50% from 1000 to 1300 nm. A reduction in crystallinity with increasing μc-Si:H layer thickness was previously observed.[21] The steep decrease in I_C^{RS} between 1300 and 1350 nm could be attributed to the contribution of the amorphous n-layer. After that, to achieve a homogeneous crystallinity across the absorber layer, the SC was stepwise adjusted during the growth of the intrinsic absorber layer, as shown in Fig. S1. This adapted deposition process will be denoted as SC profiling hereafter. The resulting Raman crystallinity depth profile is presented in Fig. 5 (red squares). The data show that SC profiling could effectively lead to a flattening of the crystallinity profile over the entire cell thickness. It is also evident in Fig. 5 that our approach to maintain a homogeneous crystallinity could be applied in the case of thinner absorber layers. Overall, with this adapted deposition process the efficiency of the solar cell could be enhanced (in the case of particular cells studied here – from 7.2 to 7.6%) along with a gain in V_{OC} (up to 20 mV). The detailed *J–V* characteristics are shown in Fig. S2, where both solar cells were made with Ag back contact.

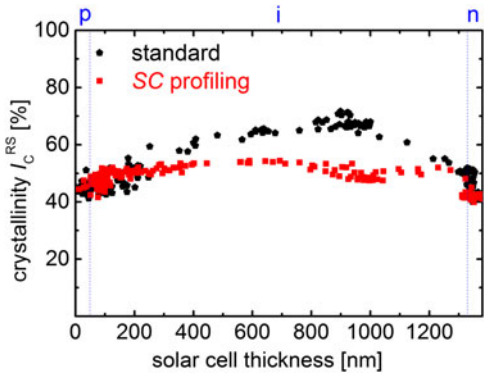

FIG. 5. Raman crystallinity depth profile of the μc-Si:H p–i–n solar cell structure without profiling of the SC (standard, black dots) and with profiling of the SC (SC profiling, red squares) during the deposition of the 1300 nm thick intrinsic absorber layer, respectively.

c. Buffer layer incorporation

This section addresses the effects of an intrinsic amorphous buffer layer at the n–i interface on the performance of the μc-Si:H solar cell, as schematically shown in the left part of Fig. 6. Similar approaches led to an increase in V_{OC} and efficiency.[30,31] However, these studies have dealt with microcrystalline buffer layers at the p–i interface. The implementation of an amorphous buffer layer at the p–i interface would however hinder the crystalline growth of the subsequent intrinsic μc-Si:H absorber layer, which is why this concept was not applied in this study. Here, n–i buffer layers of different thicknesses were incorporated in solar cells with different absorber layer thicknesses. The right part of Fig. 6 shows the V_{OC} as a function of the buffer layer thickness (5, 10, 20, 30, 50, 80 nm) for different μc-Si:H absorber layer thicknesses (1300, 650, 450 nm). The buffer layer thickness was estimated based on calculated deposition rate of buffer layer, giving an error in thickness determination within ±10%. The SC of 5% and corresponding crystalline volume fraction were kept constant for all investigated μc-Si:H solar cells. It is apparent that V_{OC} increases with increasing buffer layer thickness. Moreover, as the increase in V_{OC} is more pronounced for thinner cells, the effect of the buffer layer on the solar cell performance seems to increase with decreasing cell thickness. In this regard, it is known that the properties of the solar cell become more interface-sensitive when the cell thickness is reduced.[31] The 1300 nm thick solar cells exhibit a maximum V_{OC} of 540 mV, 650 nm thick cells exhibit up to 568 mV, and 450 nm thick cells even promote 603 mV. However, as shown in Fig. S3, for solar cells with 80 nm thick buffer layers the conversion efficiency strongly decreases. This is mainly due to poor fill factors, as the current is only slightly affected by an increase of the buffer layer thickness. Overall, the optimal buffer layer thickness, in terms of V_{OC} and efficiency could experimentally be identified for each particular solar cell thickness (Fig. S3). The 1300 nm thick solar cell shows the best performance with a buffer layer thickness of 50 nm, the optimal buffer layer thickness for the 650 nm thick cell was 20 and 5 nm buffer layer thickness exhibited the best performance in the 450 nm thick cell.

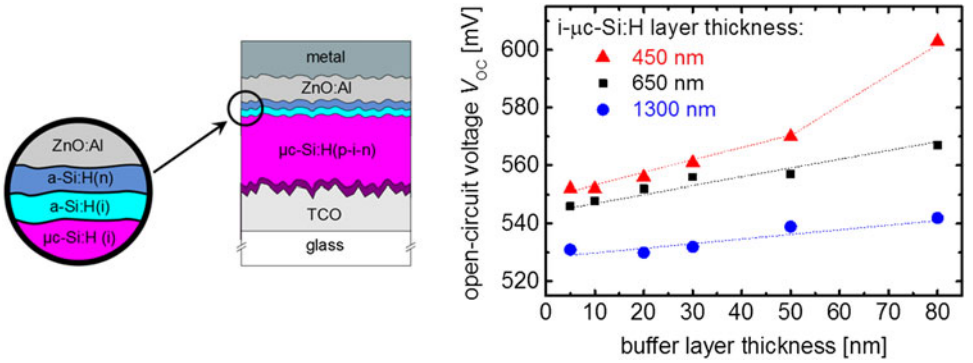

FIG. 6. Left: Schematic drawing of the μc-Si:H solar cell with the incorporated n–i buffer layer. Right: Open-circuit voltage V_{OC} of μc-Si:H solar cells as a function of n–i buffer layer thickness (5, 10, 20, 30, 50, 80 nm) for different intrinsic μc-Si:H absorber layer thicknesses (blue circles: 1300 nm, black squares: 650 nm, red triangles: 450 nm). All absorber layers were deposited at a SC of 5%. The maximum error in determination of V_{oc} is below 5 mV.

Figure 7 summarizes all presented routes discussed above and shows the conversion efficiency (η), fill factor (FF), and short-circuit current (J_{SC}) plotted versus V_{OC} for six series of depositions labeled "1300 nm", "650 nm", "450 nm", "1300 nm + SC profiling + buffer layer (50 nm)", "650 nm + buffer layer (20 nm)", and "450 nm + buffer layer (5 nm)". The range of *J*–*V* values in each series was obtained by varying the I_C^{RS}, i.e., the SC at which the intrinsic absorber layer was deposited, as already discussed in Sec. III. A. 1. a. The measured *J*–*V* data at the best-cell V_{OC} are stated in the legend of Fig. 7. For the 1300 nm series, the SC was varied between 4.4 and 6.0%, which resulted in a broad V_{OC} range of 490–620 mV, in agreement with results shown in Fig. 4. Maximum solar energy conversion efficiency is obtained for a V_{OC} of 528 mV, with a SC of 5.0%. Here, a further increase in crystallinity, i.e., decrease of SC to 4.4% could not lead to a further increase of J_{SC} and η slightly decreased along with the FF and V_{OC}. In the range of V_{OC} values between 500 and 530 mV, J_{SC} continuously decreases from around 21 mA/cm^2 down to around 10 mA/cm^2 with increasing SC from 5.0 to 5.6%. By increasing SC the μc-Si:H material increasingly becomes amorphous and therefore the current decreases. As the FF and V_{OC} mainly remain constant, the conversion efficiency and current trends in this data region resemble. In the 530–620 mV region, SC is varied between 5.6 and 6.0%, inducing a largely amorphous growth of the absorber layer, which is confirmed by the strong increase in V_{OC}. J_{SC} remains at low values between 10 and 8 mA/cm^2 and the FF strongly decreases down to 55%, indicating a reduction in the electronic quality of the material. The 650 and 450 nm series depict the PV parameters for decreased absorber layer thicknesses. Compared to the 1300 nm series, both series show increased best-cell V_{OC} values of 545 mV for 650 nm and 565 mV for 450 nm. For the 650 nm series, J_{SC} and FF values stayed nearly constant, resulting in a best conversion efficiency within a series of 8.6%. The SC profiling and buffer layer concept was simultaneously applied for the 1300 nm thick solar cells. Hereby, the best-cell V_{OC} could be increased from 528 to 551 mV, along with an increased conversion efficiency from 8.0 to 8.2%. The 650 nm thin solar cells with an incorporated 20 nm buffer layer exhibit a best-cell V_{OC} of 570 mV with 8.1% conversion efficiency. The highest best-cell V_{OC} of 580 mV is promoted by the 450 nm thin solar cells with a 5 nm buffer layer incorporated. The light absorption of these very thin cells is however rather low, which is in agreement with reduced current density of 17 mA/cm^2 and conversion efficiency of 6.7%. Overall, our results indicate that implementation of the concepts described above can lead to improved V_{OC} values over 560 mV without deterioration of other *J*–*V* characteristics.

2. a-Si:H/μc-Si:H tandem junction solar cells

The optimized, high open circuit voltage, μc-Si:H solar cells from the "1300 nm + SC profiling + buffer layer (50 nm)", "650 nm + buffer layer (20 nm)", and "450 nm + buffer layer (5 nm)" series were subsequently utilized as bottom cells in a-Si:H/μc-Si:H tandem junction solar cells. As a reference bottom cell, the "1300 nm" series was used. Various combinations of the top and bottom cells, along with corresponding absorber layer parameters and PV device parameters (η, V_{OC}, FF, J_{SC}) are listed in Table I. Since efficient hydrogen production requires solar cells, i.e., photoelectrodes, which provide a high photocurrent and operate near its maximum power point (MPP) during photoelectrochemical water splitting, the MPP voltage values (V_{MPP}) for all tandem cells are also included in Table I. The corresponding *J*–*V* characteristics are presented in Fig. 8.

As can be deduced from the data in Table I, the optimization of the μc-Si:H bottom cell could effectively

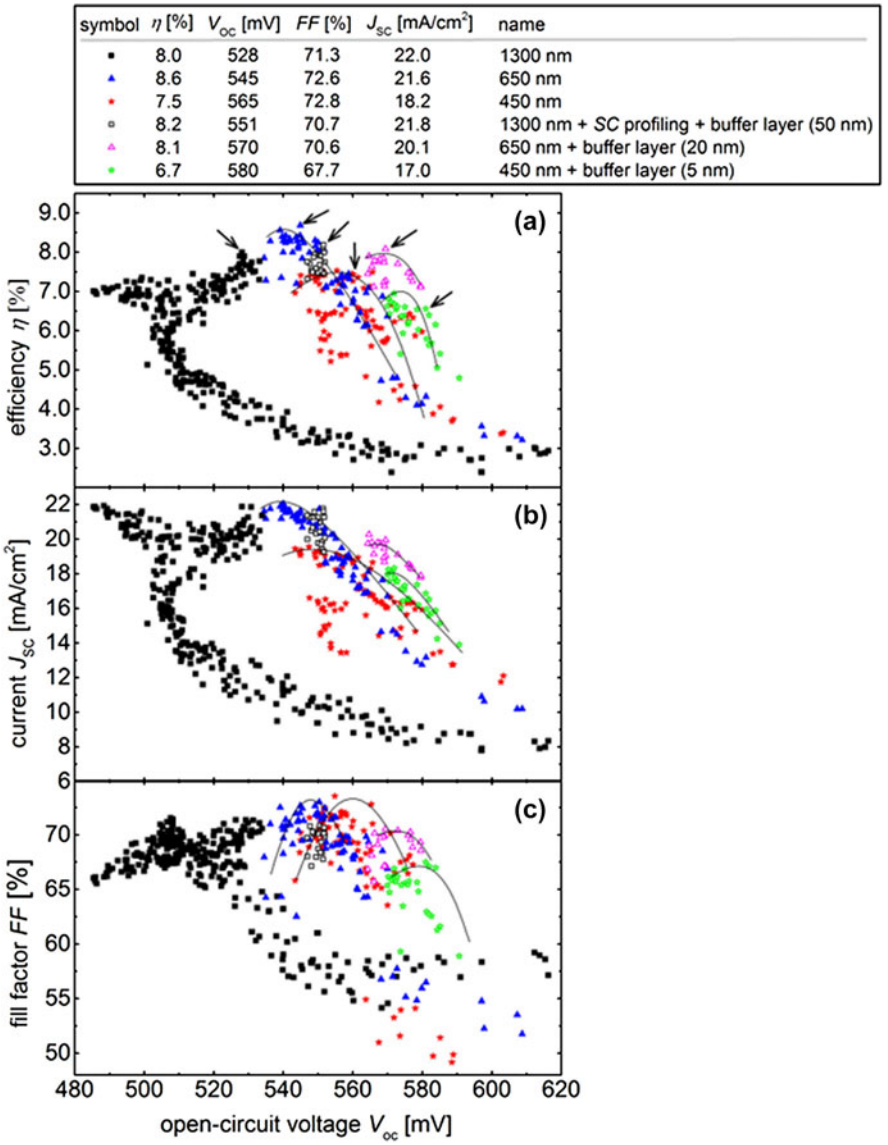

FIG. 7. Solar cell parameters: (a) conversion efficiency η, (b) short-circuit current density J_{SC}, and (c) fill factor FF versus the open-circuit voltage V_{OC} in a 1300 nm (filled squares), a 650 nm (filled triangles), and a 450 nm thick μc-Si:H absorber layer series (filled stars), in a 1300 nm thickness combined with SC profiling and incorporated buffer layer (50 nm) series (open squares), in a 650 nm thickness combined with incorporated buffer layer (20 nm) series (open triangles), and in a 450 nm thickness combined with incorporated buffer layer (5 nm) series (open stars). The trends of the six series around the best-cell V_{OC} are indicated by solid lines as a guide to the eye. The legend summarizes the best-cell parameters for the solar cells indicated by arrows in (a).

TABLE I. PV parameters of a-Si:H/μc-Si:H tandem junction solar cells fabricated with different series of μc-Si:H bottom cells and a-Si:H top cells for different SCs and thicknesses. The corresponding current–voltage measurements are depicted in Fig. 8.

	μc-Si:H bottom cell		a-Si:H top cell						
Tandem cell	Series	SC (%)	Thickness (nm)	SC (%)	η (%)	V_{oc} (mV)	FF (%)	J_{SC} (mA/cm²)	V_{mpp} (mV)
A	1300 nm	5	400	4.0	10.9	1390	72.3	10.8	1115
B	1300 nm + SC profiling + buffer layer (50 nm)	5	400	4.0	10.5	1474	65.6	10.9	1184
C	650 nm + buffer layer (20 nm)	5.3	250	4.0	11.0	1504	73.0	10.0	1255
D	450 nm + buffer layer (5 nm)	5.3	150	4.0	9.7	1515	76.2	8.4	1259

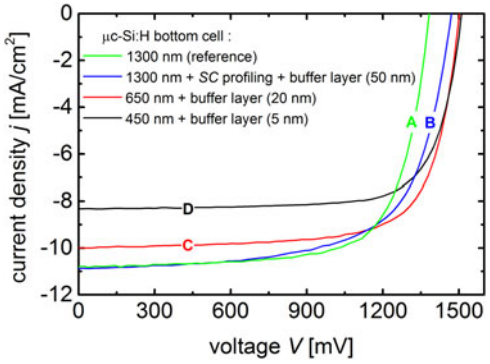

FIG. 8. Current–voltage *J*–*V* measurements of a-Si:H/μc-Si:H tandem solar cells with different μc-Si:H bottom cells: "1300 nm" reference series (cell A, green curve), "1300 nm + SC profiling + buffer layer (50 nm)" series (cell B, blue curve), "650 nm + buffer layer (20 nm)" series (cell C, red curve), and "450 nm + buffer layer (5 nm)" series (cell D, black curve). The maximum error in determination of η is below 0.2%.

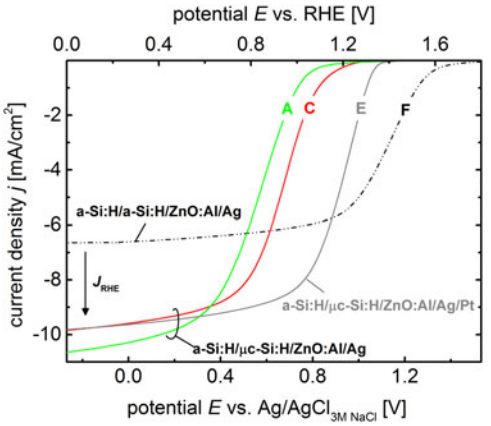

FIG. 9. Linear sweep voltammetry measurements of a-Si:H/μc-Si:H with standard ZnO:Al/Ag back contact (photocathode A and C), with ZnO:Al/Ag/Pt back contact (photocathode E), and a-Si:H/a-Si:H-ZnO/Ag (photocathode F) based photocathodes in 0.1 M H_2SO_4 solution under 100 mW/cm^2 illumination intensity at a scan rate of 30 mV s^{-1}. Photovoltaic and photoelectrochemical parameters are listed in Table II.

increase the V_{OC} and the V_{MPP} compared to the reference 1300 nm series without significantly impairing device efficiency. For the 650 nm series with incorporated buffer layer (20 nm), the efficiency could even be maintained at 11% (cell C) along with a 100 mV increase in both, V_{OC} and V_{MPP}, and a total tandem cell thickness below 1 μm. The combination of the SC profiling concept and the buffer layer incorporation in the 1300 nm series (cell B) lead to an increase in J_{SC} and V_{OC} of 0.1 mA/cm^2 and 80 mV, respectively. However, the fill factor of this tandem cell decreased to 65.6%, resulting in a V_{MPP} of 1184 mV and an overall efficiency of 10.5%. The tandem cell with the 450 nm thin bottom cell with incorporate buffer layer (cell D) exhibited the highest V_{OC} and FF values. However, due to the decreased thickness of the subcells (total tandem cell thickness was only 700 nm) J_{SC} and efficiency decreased.

B. Photoelectrochemical measurements

The tandem junction solar cells were measured as photocathodes in a three-electrode PEC measurement setup by means of linear sweep voltammetry measurement. From this measurement, the onset potential for cathodic current (E_{onset}) and the photocurrent density at 0 V versus the reversible hydrogen electrode RHE (J_{RHE}), which can be correlated with the V_{OC} and the J_{SC} of the solar cell, respectively, were determined for the photocathodes. In Fig. 9, the photoelectrochemical performance of the a-Si:H/μc-Si:H tandem cell with the 650 nm thin bottom cell with a 20 nm buffer layer (photocathode C in Table II, red curve) is compared to the a-Si:H/μc-Si:H reference tandem cell (photocathode A in Table II, green curve). The corresponding PV and PEC parameters are listed in Table II. The data evidences that PV and photoelectrochemical performances show the same trends:

TABLE II. PV (V_{OC}, J_{SC}) and PEC parameters (E_{onset}, J_{RHE}) of a-Si:H/μc-Si:H photocathodes with standard ZnO:Al/Ag back contacts (photocathode A and C, compare with Table I) and with ZnO:Al/Ag/Pt back contacts (photocathode E). Additionally, the parameters of an a-Si:H/a-Si:H photocathode are shown (photocathode F). The onset potential of cathodic current, E_{onset}, was taken as the value at a photocurrent density of −0.5 mA/cm^2 from Fig. 9.

Photocathode	V_{oc} (mV)	J_{SC} (mA/cm^2)	E_{onset} (mV versus RHE)	J_{RHE} (mA/cm^2)
A (1300 nm series)	1390	10.8	1042	10.7
C (650 nm + buffer layer series)	1504	10.0	1141	9.9
E (same as C with 50 nm Pt)	...	...	1327	9.9
F (a-Si:H/a-Si:H)	1852	6.8	1562	6.8

the higher the V_{OC} and J_{sc} of a solar cell, the higher is its E_{onset} and J_{RHE} as a photocathode. Still, there is a disparity in V_{OC} and E_{onset} values. This difference can be correlated with the overpotential for the HER. Notwithstanding this, the optimized a-Si:H/μc-Si:H tandem-based photocathode (photocathode C) showed a 100 mV increase in E_{onset} compared to the reference tandem photocathode (photocathode A) and exhibited 1141 mV versus RHE, along with a J_{RHE} of 9.9 mA/cm^2.

To fully explore the performance of the photocathode, platinum was evaporated on the ZnO:Al/Ag back contact to act as a catalyst on the electrolyte side (photocathode E in Table II, gray curve). Here, no effect on J_{RHE} is observed, proving that the optics of the photocathode back contact remain mainly unaffected by the thin platinum layer. However, with respect to the ZnO:Al/Ag back contact photocathode, the photocathode with ZnO:Al/Ag/Pt back contact shows a significant

shift in E_{onset} in positive bias direction and is measured to be 1327 mV versus RHE. This result evidences both the excellent catalytic activity of platinum as a catalyst for the HER and its viable combination with the a-Si:H/μc-Si:H/ZnO:Al/Ag tandem device.

To underline the difference between a-Si:H/μc-Si:H and a-Si:H/a-Si:H tandem junction solar cells, Fig. 9 additionally shows the linear sweep voltammetry measurement of an a-Si:H/a-Si:H based photocathode (photocathode F in Table II, dotted black curve), which will be discussed in the next section. The development and application of a-Si:H/a-Si:H photocathodes with platinum catalyst are discussed in detail in Ref. 20.

IV. DISCUSSION

Although thin film silicon-based devices, in particular a-Si:H multijunction solar cells, are among the most suitable candidates for efficient water splitting,[10,12,14] there is a tradeoff between high open-circuit voltages and high photocurrents. The presented routes of high V_{OC} development, particularly the reduction of the intrinsic μc-Si:H absorber layer thickness, SC profiling, and buffer layer incorporation distinctly contributed to the closure of this high voltage/high current gap and considerably improved V_{OC} in a-Si:H/μc-Si:H tandem junction solar cells, which provide significantly higher photocurrents as their all-amorphous counterparts. Thickness reduction effectively enhanced V_{OC}. In μc-Si:H solar cells, V_{OC} is limited by the bulk recombination in the absorber layer.[32,33] Decreasing the thickness of this layer will therefore lead to an increase in V_{OC} due to the reduced volume. Additionally, J_{SC} and FF were only slightly affected, which resulted in an increased conversion efficiency for solar cells with an intrinsic μc-Si:H layer thickness of 650 nm. The highest V_{OC} values were achieved for 450 nm thin absorber layers, but the current densities decreased, as the absorption was drastically lowered. The implementation of the SC profiling and buffer layer concept then could further increase V_{OC} for all cell thicknesses and thus maintain conversion efficiencies above 8% for the 1300 and 650 nm thick cells and around 7% for the 450 nm thick cells. SC profiling ensures a homogeneous and moderate crystallinity level across the entire μc-Si:H absorber layer. The buffer layer at the n–i interface presumably acts as a defect passivation layer and reduces interface recombination, as already reported for heterojunction solar cells.[34,35]

The best high voltage/high current tradeoff was provided by the a-Si:H/μc-Si:H tandem cell constituted of a 650 nm thick μc-Si:H bottom cell with a 20 nm buffer layer and a 250 nm thick a-Si:H top cell (cell C in Table I), which promoted over 1.5 V and 10.0 mA/cm^2 with 11.0% conversion efficiency. Furthermore, this tandem cell had a total thickness below 1 μm, accentuating its low-cost production and potential high stability against light-induced degradation.[36]

Figure 10 presents the QEs for the a-Si:H/μc-Si:H tandem solar cell series (same as in Table I). By decreasing the top and the bottom cell thickness, the current densities of the top and bottom cells, $J_{SC,top}$ and $J_{SC,bot}$, decrease while V_{OC} increases (see Table I and Fig. 8). As the reduction of the top cell thickness is accompanied with a higher transparency, more light can enter the bottom cell. This is confirmed by the increase of the bottom cell QE in the wave length range between 400 and 600 nm with decreasing μc-Si:H absorber layer thickness (indicated by arrow in Fig. 10). This might explain the relatively high photocurrent of tandem cell B of 10.0 mA/cm^2 with the 650 nm bottom cell compared to tandem cell A with the 1300 nm bottom cell, which provides 10.8 mA/cm^2.

The photoelectrochemical characterization revealed that PV and PEC parameters of the solar cells and photocathodes, respectively, are correlated. Short-circuit current densities J_{SC} and J_{RHE} are not affected, however V_{OC} and E_{onset} significantly differ because of overpotential losses. For the particular investigated system in this study, including the silicon photocathode with the ZnO:Al/Ag back contact and 0.1 M H_2SO_4 electrolyte solution, the HER overpotential was around 350 mV for all investigated photocathodes (at −0.5 mA/cm^2), as can be extracted from Table II. In general, the overall performance of the tandem solar cell is reduced when applied as a photocathode in the PEC arrangement. This is mainly due to overpotential losses and mass transport limitations caused by the low conductivity of the herein used electrolyte which

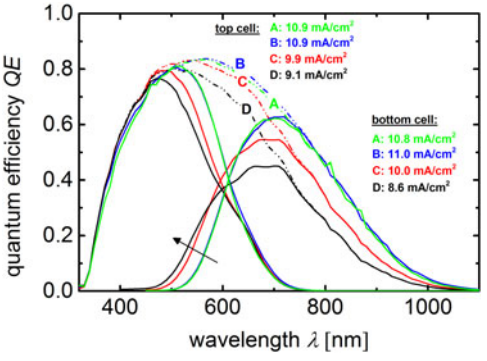

FIG. 10. Quantum efficiency measurements of the four a-Si:H/μc-Si:H tandem junction solar cells from Table I. Letter A denotes the "1300 nm" reference series (green curves), B the "1300 nm + SC profiling + buffer layer (50 nm) series" (blue curves), C the "650 nm + buffer layer (20 nm)" series (red curves), and D the "450 nm + buffer layer (5 nm)" series (black curves). The current densities of the top and bottom cells, $J_{SC,top}$ and $J_{SC,bot}$ are depicted in the figure. Letters A–D indicate tandem cells listed in Table I. Arrow indicates the trend of increasing bottom cell QE in the wave length range between 400 and 600 nm with decreasing μc-Si:H absorber layer thickness. The top and bottom cell current densities calculated from the QE-curves are placed near the related measurements. The maximum error in determination of J_{QE} is below 0.05 mA/cm^2.

enforces an additional resistance on the charge transport.[37] The related sinusoidal-like shape of the linear sweep curves (Fig. 9) is related to the reduced fill factor of the whole PEC device. In this regard, the application of different electrolyte solutions, which could reduce the electrolyte resistance, need to be tested for improving the a-Si.H/μc-Si:H photocathode performance. Nevertheless, by depositing a thin layer of platinum on the back contact, overpotential losses could be reduced by about 200 mV (Table II) and the corresponding a-Si:H/μc-Si:H photocathode exhibited an E_{onset} of 1327 mV versus RHE. One of the most recent works focusing on the direct application of thin film silicon solar cells as photoelectrodes was done by Lin et al.[11] Here, single junction a-Si:H solar cells were tested as photocathodes under the irradiation by a simulated sunlight (AM 1.5 light spectrum, 100 mW/cm^2) and exhibited an E_{onset} of 0.93 V versus RHE and photocurrent densities of 6.1 mA/cm^2 at 0.8 versus RHE, respectively. The a-Si:H/μc-Si:H photocathodes with Pt as a catalyst, investigated in this study, promoted a photocurrent density of 8.3 mA/cm^2 at 1.0 V versus RHE, proving a significant improvement in the photocathode performance.

As already pointed out, efficient bias-free solar water splitting requires photocathodes with high photovoltages in combination with high photocurrent densities.[4,5] Although the a-Si:H/a-Si:H photocathode, shown in Fig. 9, exhibits a high E_{onset} over 1.56 V versus RHE, and is therefore suitable for self-contained water splitting (including overpotentials),[8,20] the photocurrent density is low compared to the a-Si:H/μc-Si:H photocathodes, which limits the overall water splitting efficiency. The a-Si:H/μc-Si:H based photocathodes provide significantly higher photocurrents (Table II and indicated in Fig. 9), but the lower photovoltages only allow for small overpotential losses, and thus, for the use of precious-metal catalysts. In this regard, the hydrogen production via splitting of different acidic electrolyte solutions, like hydriodic acid (HI) or hydrobromic acid (HBr) may be advantageous for a-Si:H/μc-Si:H based PEC devices. The corresponding thermodynamic potentials for hydrogen decomposition via electrolysis are lower than 1.23 V,[38] namely 1.07 and 0.54 V for HBr and HI splitting, respectively.

V. CONCLUSION

We presented the development of a-Si:H/μc-Si:H tandem junction solar cells for the application in photoelectrochemical water splitting devices for hydrogen production. The optimization of the individual μc-Si:H single junction solar cells with focus on high open-circuit voltage, led to a 100 mV increase in V_{OC}, while maintaining the device efficiency. The best a-Si:H/μc-Si:H tandem junction solar cell provided over 1.5 V and a conversion efficiency of 11% with a total silicon layer thickness below 1 μm.

The performance of the developed tandem junction solar cells as photocathodes was demonstrated in a PEC arrangement. In particular, the a-Si:H/μc-Si:H photocathodes with a ZnO:Al/Ag/Pt back contact exhibited a high photocurrent density of 9.9 mA/cm^2 at 0 V versus RHE and an onset potential over 1.3 V versus RHE, and thus, fulfill the main thermodynamic requirement for water electrolysis. This result provides evidence that a-Si:H/μc-Si:H based PEC systems can offer a pathway toward low-cost and efficient devices for solar hydrogen generation.

Conflict of Interest

The authors declare that there is no conflict of interest regarding the publication of this paper.

ACKNOWLEDGMENTS

We thank K. Wilken, S. Tillmanns, L. Petter, W. Reetz, H. Siekmann, U. Gerhards, M. Hülsbeck, and A. Lambertz for their contributions to this work. The research is partly financially supported by the Deutsche Forschungsgemeinschaft (DFG) Priority Programme 1613: Regeneratively produced fuels by light driven water splitting: Investigation of involved elementary processes and perspectives of technologic implementation, and by the Bundesministerium für Bildung und Forschung (BMBF) in the network project: Sustainable Hydrogen (FKZ 03X3581B).

REFERENCES

1. E. Miller: *White Papers on Materials for Photoelectrochemical Water Splitting* (DOE PEC Working Group, Washington, DC, 2013).
2. C.A. Grimes, O.K. Varghese, and S. Ranjan: *Light, Water, Hydrogen: The Solar Generation of Hydrogen by Water Photoelectrolysis* (Springer, New York, 2008).
3. Z. Li, W. Luo, M. Zhang, J. Feng, and Z. Zou: Photoelectrochemical cells for solar hydrogen production: Current state of promising photoelectrodes, methods to improve their properties, and outlook. *Energy Environ. Sci.* **6**, 347–370 (2013).
4. M.F. Weber and M.J. Dignam: Splitting water with semiconducting photoelectrodes - Efficiency considerations. *Int. J. Hydrogen Energy* **11**(4), 225–232 (1986).
5. A.J. Nozik: Photoelectrochemistry: Applications to solar energy conversion. *Ann. Rev. Phys. Chem.* **29**, 189–222 (1978).
6. O. Khaselev and J.A. Turner: A monolithic photovoltaic-photoelectrochemical device for hydrogen production via water splitting. *Science* **280**(5362), 425–527 (1998).
7. O. Khaselev, A. Bansal, and J.A. Turner: High-efficiency integrated multijunction photovoltaic/electrolysis systems for hydrogen production. *Int. J. Hydrogen Energy* **26**(2), 127–132 (2001).
8. S. Licht, B. Wang, S. Mukerji, T. Soga, M. Umeno, and H. Tributsch: Over 18% solar energy conversion to generation of hydrogen fuel; theory and experiment for efficient solar water splitting. *Int. J. Hydrogen Energy* **26**, 653–659 (2001).

9. T.J. Jacobsson, V. Fjällström, M. Sahlberg, M. Edoff, and T. Edvinsson: A monolithic device for solar water splitting based on series interconnected thin film absorbers reaching over 10% solar-to-hydrogen efficiency. *Energy Environ. Sci.* **6**, 3676 (2013).
10. F.F. Abdi, L. Han, A.H.M. Smets, M. Zeman, B. Dam, and R. van de Krol: Efficient solar water splitting by enhanced charge separation in a bismuth vanadate-silicon tandem photoelectrode. *Nat. Commun.* **4**, 2195 (2013).
11. Y. Lin, C. Battaglia, M. Boccard, M. Hettick, Z. Yu, C. Ballif, J.W. Ager, and A. Javey: Amorphous Si thin film based photocathodes with high photovoltage for efficient hydrogen production. *Nano Lett.* **13**(11), 5615–5618 (2013).
12. L. Han, F.F. Abdi, P. Perez Rodriguez, B. Dam, R. van de Krol, M. Zeman, and A.H.M. Smets: Optimization of amorphous silicon double junction solar cells for an efficient photoelectrochemical water splitting device based on a bismuth vanadate photoanode. *Phys. Chem. Chem. Phys.* **16**, 4220–4229 (2014).
13. S.Y. Reece, J.A. Hamel, K. Sung, T.D. Jarvi, A.J. Esswein, J.J.H. Pijpers, and D.G. Nocera: Wireless solar water splitting using silicon-based semiconductors and earth-abundant catalysts. *Science* **334**, 645–648 (2003).
14. R.E. Rocheleau, E.L. Miller, and A. Misra: High-efficiency photoelectrochemical hydrogen production using multijunction amorphous silicon photoelectrodes. *Energy Fuels* **12**(1), 3–10 (1998).
15. W. Calvet, E. Murugasen, J. Klett, B. Kaiser, W. Jaegermann, F. Finger, S. Hoch, M. Blug, and J. Busse: Silicon based tandem cells: Novel photocathodes for hydrogen production. *Phys. Chem. Chem. Phys.* **16**, 12043–12050 (2014).
16. A. Shah: *Thin-Film Silicon Solar Cells, Photovoltaics and Large-area Electronics* (Crc Pr Inc., Lausanne, Switzerland, 2008).
17. H. Keppner, J. Meier, P. Torres, D. Fischer, and A. Shah: Microcrystalline silicon and micromorph tandem solar cells. *J. Appl. Phys.* **A69**, 169 (1999).
18. S. Klein, F. Finger, R. Carius, T. Dylla, B. Rech, M. Grimm, L. Houben, and M. Stutzmann: Intrinsic microcrystalline silicon prepared by hot-wire chemical vapour deposition for thin film solar cells. *Thin Solid Films* **430**(1–2), 202–207 (2003).
19. W. Böttler, V. Smirnov, J. Hüpkes, and F. Finger: Texture-etched ZnO as a versatile base for optical back reflectors with well-designed surface morphologies for application in thin film solar cells. *Phys. Status Solidi A* **209**(6), 1144–1149 (2012).
20. F. Urbain, K. Wilken, V. Smirnov, O. Astakhov, A. Lambertz, J-P. Becker, U. Rau, J. Ziegler, B. Kaiser, W. Jaegermann, and F. Finger: Development of thin film amorphous silicon tandem junction based photocathodes providing high open-circuit voltages for hydrogen production. *Int. J. Photoenergy* **2014**, 249317 (2014).
21. L. Houben, M. Luysberg, P. Hapke, R. Carius, F. Finger, and H. Wagner: Structural properties of microcrystalline silicon in the transition from highly crystalline to amorphous growth. *Philos. Mag. A* **77**(6), 1447 (1998).
22. F. Köhler, S. Schicho, B. Wolfrum, A. Gordijn, S.E. Pust, and R. Carius: Gradient etching of silicon-based thin films for depth-resolved measurements: The example of Raman crystallinity. *Thin Solid Films* **520**(7), 2605–2608 (2012).
23. V. Smirnov, C. Das, T. Melle, A. Lambertz, M. Hülsbeck, R. Carius, and F. Finger: Improved homogeneity of microcrystalline absorber layer in thin-film silicon tandem solar cells. *Mater. Sci. Eng., B* **159–160**, 44–47 (2009).
24. A. Lambertz, V. Smirnov, T. Merdzhanova, K. Ding, S. Haas, G. Jost, R.E.I. Schropp, F. Finger, and U. Rau: Microcrystalline silicon–oxygen alloys for application in silicon solar cells and modules. *Sol. Energy Mat. Sol. Cells* **119**, 134–143 (2013).
25. H. Gary: Photoelectrochemical cell measurements: Getting the basics right. *J. Phys. Chem. Lett.* **3**(9), 1208–1213 (2012).
26. O. Vetterl, F. Finger, R. Carius, P. Hapke, L. Houben, O. Kluth, A. Lambertz, A. Mück, B. Rech, and H. Wagner: Intrinsic microcrystalline silicon: A new material for photovoltaics. *Sol. Energy Mater. Sol. Cells* **62**(1–2), 97–108 (2000).
27. C. Droz, E. Vallat-Sauvain, J. Bailat, L. Feitknecht, J. Meier, and A. Shah: Relationship between Raman crystallinity and open-circuit voltage in microcrystalline silicon solar cells. *Sol. Energy Mater. Sol. Cells* **81** (1), 61–71 (2004).
28. S. Reynolds, R. Carius, F. Finger, and V. Smirnov: Correlation of structural and optoelectronic properties of thin film silicon prepared at the transition from microcrystalline to amorphous growth. *Thin Solid Films* **517**, 6392 (2009).
29. M.N. van den Donker, S. Klein, B. Rech, and F. Finger: Microcrystalline silicon solar cells with an open-circuit voltage above 600 mV. *Appl. Phys. Lett.* **90**(18), 183504 (2007).
30. Y. Mai, S. Klein, R. Carius, J. Wolff, A. Lambertz, and F. Finger: Open circuit voltage improvement of high-deposition-rate microcrystalline silicon solar cells by hot wire interface layers. *J. Appl. Phys.* **87**(7), 114913 (2005).
31. G. Bugnon, G. Parascandolo, S. Hänni, M. Stuckelberger, M. Charrière, M. Despeisse, F. Meillaud, and C. Ballif: Silicon oxide buffer layer at the p–i interface in amorphous and microcrystalline silicon solar cells. *Sol. Energy Mater. Sol. Cells* **120**, 143–150 (2014).
32. B.E. Pieters, H. Stiebig, M. Zeman, and R.A.C.M.M. van Swaaij: Determination of the mobility gap of intrinsic μc-Si:H in p-i-n solar cells. *J. Appl. Phys.* **105**, 044502 (2009).
33. T. Brammer and H. Stiebig: Applying analytical and numerical methods for the analysis of microcrystalline silicon solar cells. *Sol. Energy Mater. Sol. Cells* **90**(18–19), 3021–3030 (2006).
34. E. Centurioni, D. Iencinella, R. Rizzoli, and F. Zignani: Silicon heterojunction solar cell: A new buffer layer concept with low-temperature epitaxial silicon. *IEEE Trans. Electron Devices* **51**(11), 1818–1824 (2004).
35. M. Lu, S. Bowden, U. Das, and R. Birkmire: Interdigitated back contact silicon heterojunction solar cell and the effect of front surface passivation. *Appl. Phys. Lett.* **91**, 063507 (2007).
36. T. Repmann, B. Sehrbrock, C. Zahren, H. Siekmann, J. Müller, B. Rech, W. Psyk, R. Geyer, and P. Lechner: Thin film solar modules based on amorphous and microcrystalline silicon. *Proceedings of Third World Conference on Photovoltaic Energy Conversion*, Osaka, Japan, 2003, pp. 1574–1579.
37. R. van de Krol and M. Grätzel: *Photoelectrochemical Hydrogen Production* (Springer, New York, 2012).
38. C. Levy-Clement, A. Heller, W.A. Bonner, and B.A. Parkinson: Spontaneous photoelectrolysis of HBr and HI. *J. Electrochem. Soc.* **129**(8), 1701–1708 (1982).

Supplementary Material

To view supplementary material for this article, please visit http://dx.doi.org/jmr.2014.308.